Morphology, performance and stability of multi-bore capillary La$_{0.6}$Sr$_{0.4}$Co$_{0.2}$Fe$_{0.8}$O$_{3-\delta}$ oxygen transport membranes

Yunsi Chi[a,b], Tao Li[a,b], Bo Wang[a,b], Zhentao Wu[b,c], Kang Li[a,b,*]

[a] Barrer Centre, Imperial College London, South Kensington, SW7 2AZ London, UK
[b] Department of Chemical Engineering, Imperial College London, South Kensington, SW7 2AZ London, UK
[c] Aston Institute of Materials Research, School of Engineering and Applied Science, Aston University, Birmingham B4 7ET, UK

A B S T R A C T

Mixed ionic-electronic conducting 3, 4, 7-bore capillary membranes made of La$_{0.6}$Sr$_{0.4}$Co$_{0.2}$Fe$_{0.8}$O$_{3-\delta}$ (LSCF) were successfully prepared by the combined phase inversion/sintering technique. The membranes fabricated have asymmetric wall structures with micro-channels formed in between surfaces, and dense layers sandwiched in between the micro-channels. By changing the solvent from DMSO to NMP, changes in the morphology of the 7-bore membrane were observed, where the separation layer has reduced its effective thickness. The multi-bore membranes exhibited 3-point bending fracture loads of 10.4, 13.5, 15.4 and 11.7 N with a 3 cm testing span for the 3-bore, 4-bore, 7-bore-DMSO and 7-bore-NMP samples, respectively, which are much stronger than single-bore hollow fibre membranes. Oxygen permeation of the multi-bore membranes was measured with a sweep gas flow through lumen and the effect of operating temperature has on the performance was studied between 750 °C to 1000 °C. Oxygen fluxes measured are comparable to typical sandwich-like structured single-bore hollow fibres at temperatures below 900 °C, but are notably higher at higher temperatures owe to their thinner membrane walls. The 200-h long-term permeation test conducted on the 7-bore membrane showed a slight increase in permeation flux, but the sign of kinetic demixing/decomposition appeared on the outer surface, where the surface of the thinnest membrane walls underwent faster demixing/decomposition than the thickest walls. In summary, the results demonstrated that multi-bore configurations can achieve optimised material distribution during the fabrication, and can obtain strong mechanical property, high permeation flux for the final products whilst maintaining high membrane area to volume ratios.

1. Introduction

Oxygen production is of great importance in industrial and environmental processes. Current technologies such as the cryogenic distillation and pressure swing adsorption (PSA) are expensive and energy intensive. The search for alternate technology has led to the use of ceramic membranes for oxygen separation. Over the past 30 years, considerable efforts have focused on the use of dense ceramic membranes, especially mixed ionic-electronic conducting (MIEC) membranes capable of conducting both ions and electrons [1–4]. These MIEC membranes can theoretically produce 100% pure oxygen at elevated temperatures under oxygen partial pressure differences without the need of an external electrical circuit. As a result, these membranes offer a simplified and cost effective method for oxygen separation. Furthermore, they have attracted considerable attention for their integration with membrane reactors in reactions such as partial oxidation of methane to syngas (POM) and oxidative coupling of

methane to C$_2$ (ethylene and/or ethane) [5–9].

The performance of MIEC membranes strongly depends on the membrane material and the membrane structure. Enormous efforts have been made to tune the chemistry of the membrane material to obtain highly permeable and stable materials, an excellent review article can be found elsewhere [3]. Besides the membrane material, membrane structure is equally important for oxygen separation, therefore vast amount of research have also been undertaken to study different membrane configurations. Disk and plate membranes have been widely used in research works because of the ease of fabrication. However, membrane of this geometry possesses low separation area to volume ratio, which makes it undesirable for large scale production. Conventional tubular membranes have a larger active area compared to that of the disc membranes, but their thick dense separation layers contribute to an increased bulk diffusion resistance, resulting in low oxygen permeation flux. So far the most advanced structural design in terms of permeation rate has been the hollow fibre configuration.

Hollow fibre membranes have thin separating layers and exhibit high membrane area to volume ratios, resulting in higher oxygen permeation flux per unit volume compared to conventional disk and tubular membranes [10–16]. However, major drawbacks of hollow fibres are the weak mechanical stability from their small dimensions, which may jeopardize the robustness of membrane modules in high flowrate and high pressure operating conditions. In order to solve the mechanical stability issue, efforts have been made to optimize membrane configuration to achieve membranes with good mechanical property whilst maintaining good oxygen permeation flux. A bundling strategy has been proposed recently to improve the mechanical stability of hollow fibre membranes by using catalytic perovskite binders, which may not only increase the mechanical stability, but also increase the permeation flux owe to the catalytic activity of the binder [17]. However, such strategy adopts multi-step batch-by-batch fabrication process and needs extra cost for the binder material, therefore the whole fabrication cost is significantly increased. Alternatively, the requirement of one-step continuous production has led to the recent interest in fabricating multi-bore capillary membranes [18–21]. Results obtained from such configurations showed some promising results where they exhibited an improved mechanical property with good oxygen permeation flux for the 4-bore membranes. However, work in this field is still very limited and so far only 4-bore membranes were investigated on 3 different membrane materials, i.e., Nb_2O_5-doped $SrCo_{0.8}$ $Fe_{0.2}O_{3-\delta}$ (SCFNb), $SrFe_{0.8}Nb_{0.2}O_{3-\delta}$ (SFN) and $Ba_{0.5}Sr_{0.5}Co_{0.8}Fe_{0.2}O_{3-\delta}$ (BSCF) for oxygen separation [18–21].

Our previous study has shown successful preparation of 3, 7, 19-bore porous capillary membranes made of alumina using the combined phase-inversion and sintering method [22], and they showed not only much improved mechanical property, but also enhanced water permeation flux compared with their single-bore hollow fibre counterparts. Furthermore, both fracture load and permeation flux increased when the number of bores increased. It would be interesting to investigate the effects of different configuration MIEC multi-bore membranes have on their mechanical and permeation performances, as the knowledge from porous membranes may differ from dense membranes due to different transport mechanisms. In this study, multi-bore $La_{0.6}Sr_{0.4}Co_{0.2}Fe_{0.8}O_{3-\delta}$ (LSCF) MIEC capillary membranes with 3, 4 and 7 bores are prepared and studied. LSCF is selected as the membrane material because it possesses both good permeability and good chemical stability [23–27], furthermore, widely available literature regarding LSCF single-bore hollow fibre membranes makes it easy for comparisons. We show here that different from conventional ram extrusion, by adjusting fabrication parameters in the phase-inversion process, the morphology of multi-bore membranes can be notably altered. The mechanical property and oxygen permeation flux for the multi-bore LSCF membranes are studied, and the long-term 200 h test on stability and kinetic demixing/decomposition are also investigated with the 7-bore membrane.

2. Experimental

2.1. Materials

Commercially available $La_{0.6}Sr_{0.4}Co_{0.2}Fe_{0.8}O_{3-\delta}$ (LSCF) ceramic powder with surface area of 10.2 $m^2\,g^{-1}$ was used as the membrane material (Fuel Cell Materials, Columbus, Ohio). The polymer binder used was Polyethersulfone (PESf) (RadelA-300, Solvay Advanced Polymers GmbH, Dusseldorf, Germany). Arlacel P135 (Uniquema, Wilton, UK) was used as the dispersant and dimethyl sulfoxide (DMSO, VWR) or N-Methyl-2-pyrrolidone (NMP, VWR) was selected as the solvent. The internal and external coagulants used were deionised water.

Table 1
Ceramic suspension compositions and spinning parameters.

		3-bore	4-bore	7-bore DMSO	7-bore NMP
Suspension compositions	LSCF (wt%)	67.0			
	DMSO or NMP (wt%)	25.8			
	PESf (wt%)	6.7			
	Dispersant (wt%)	0.5			
Spinning parameters	Dope extrusion rate ($cm^3\,min^{-1}$)	9	9	8	9
	Bore liquid (water) rate ($cm^3\,min^{-1}$)	12	14	14	18
	Air gap (cm)	0	0	0	1

2.2. Multi-bore capillary membrane fabrication

The LSCF multi-bore capillary membranes were fabricated using the combined phase inversion/sintering method and the compositions of ceramic suspension are listed in Table 1. The ceramic suspension was mixed thoroughly by ball milling prior to removing air bubbles using the vacuum system, and then spun through a specially designed spinneret to obtain the multi-bore capillary membrane precursors. In this study, triple, tetra and seven-bore spinnerets were used, whose geometric configurations are shown in Fig. 1. For the 3-bore and 4-bore membranes, DMSO was used as the solvent for the ceramic suspension; for the 7-bore membranes, two types of suspension were used, in which DMSO or NMP was the solvent, and the obtained membrane will be named as 7-bore-DMSO and 7-bore-NMP in the following sections, respectively. The spinning parameters used to obtain the multi-bore capillary membranes are also summarised in Table 1. After drying, the precursors were then heated to 600 °C at a rate of 2 °C min^{-1} and then stayed at this temperature for 2 h to remove the polymer binder, followed by sintering at 1350 °C for 5 h with a heating rate of 3 °C min^{-1}. Finally, the furnace was cooled at a rate of 3 °C min^{-1} to room temperature.

2.3. Oxygen permeation test

The shell side of the membrane was exposed to ambient air and the sweep gas argon was fed through the capillary bores creating the oxygen partial pressure difference for oxygen permeation. The flowrate of the sweep gas was maintained at 100 cm^3 min^{-1} throughout the experiment. The oxygen permeated was carried by the sweep gas and measured by gas chromatography (GC, Varian 3900). The oxygen permeation flux was calculated using the below equation:

$$J_{O_2} = \frac{V_{Ar}\,y_{O_2}}{A_o\,(100 - y_{O_2})} \tag{1}$$

where J_{O_2} is the oxygen permeation flux, V_{Ar} is the volumetric flowrate of the argon sweep gas, A_o is the outer membrane surface area, y_{O_2} is the percentage oxygen concentration detected by the GC. The data were collected within a time window of 30 min after the temperature became stable, and a stable flux with an error less than 2% is reported within 2 h.

2.4. Characterisation

Morphologies of the multi-bore capillary membranes were studied using the Gemini LEO 1525 field emission gun scanning electron microscope (SEM). The mechanical property was evaluated using the three-point bending method by an Instron materials testing system (Model 5544) with a 5 kN load cell, the samples were positioned with a span of 30 mm onto the sample holder. A minimum of 5 samples were tested and the average value with an error less than 15% is reported.

Fig. 1. Configuration of 3, 4 and 7-bore spinnerets.

3. Results and discussions

3.1. Macrostructure of the multi-bore capillary membranes

The 3, 4, 7-bore capillary membranes were successfully fabricated by the combined phase-inversion and sintering method. SEM images of the cross sectional area are shown in Fig. 2. The dimensions of the sintered multi-bore membranes are listed in Table 2. It can be seen with the same suspension composition and similar fabrication parameters, in general the outer diameter of the capillary membrane increases with the number of bores, although the multi-bore spinnerets used here have the same designed outer and bore diameters. This is because when the number of bores increases, the overall precipitation rate of the suspension would be increased due to the reduced wall thicknesses and the more evenly distributed interior coagulant. Therefore this resists the elongation from gravity of the nascent membranes that would otherwise reduce the outer diameter. And in general, the thickness of the thinnest walls between the bores and the outer surface reduces, which is concurrent with the design of the spinnerets. For the 7-bore capillary membranes with the same spinneret configuration, changing the solvent in the suspension from DMSO to NMP has caused considerable impacts to the cross-sectional morphology and distribution of the membrane material. For the 7-bore-NMP case, the bore liquid flowrate had to be increased during the fabrication to obtain fully open bores. Therefore, the walls between the outer surface and bores became thinner and more flattened compared
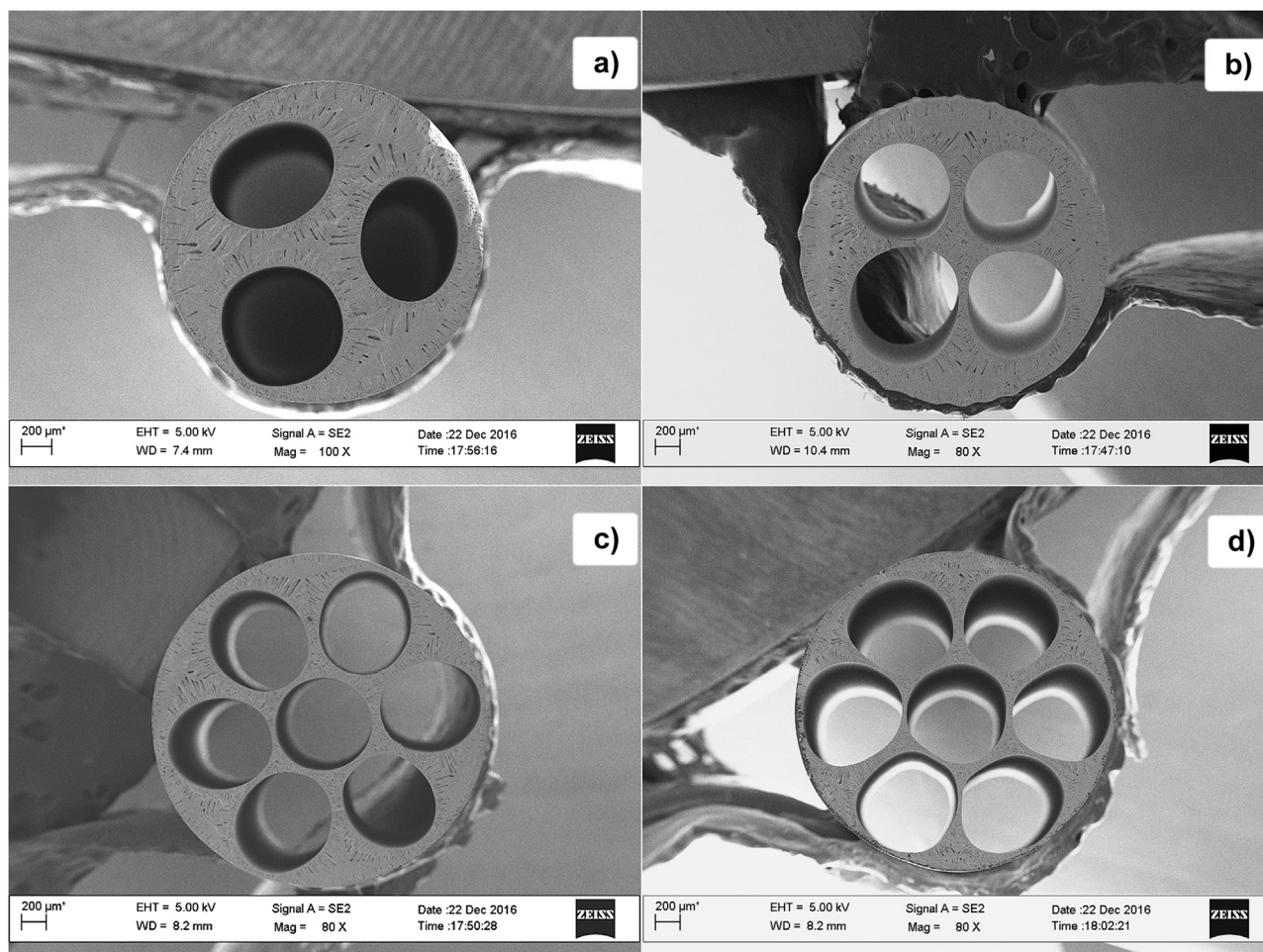

Fig. 2. Cross-sectional SEM images of sintered (a) 3-bore, (b) 4-bore, (c) 7-bore-DMSO and (d) 7-bore-NMP LSCF capillary membranes.

Table 2
Dimensions of sintered multi-bore capillary membranes and the theoretical outer surface area to volume ratios.

Membrane	Outer diameter (mm)	Average bore diameter (mm)	Average bore centre to capillary centre distance (mm)[a]	Average thickness of thinnest walls (μm)	Outer surface area to volume ratio (m² m⁻³)
3 – bore	2.12	0.73	0.55	130	1711
4 – bore	2.41	0.81	0.61	80	1505
7 – bore – DMSO	2.60	0.77	0.83	50	1395
7 – bore – NMP	2.52	0.78	0.81	30	1440

[a] Only outer 6 bores are counted for the 7-bore membranes.

to the 7-bore-DMSO membrane due to the greater interior hydraulic pressure. Furthermore, the outer diameter of the 7-bore-NMP membrane became smaller than the 7-bore-DMSO membrane due to the greater elongation effect. The impact of NMP solvent has on the morphology can be attributed to its higher solvent power to PESf compared to DMSO, which leads to a slower precipitation rate of the polymer binder in the suspension [28], and therefore the nascent membranes have less resistance to deformation by hydraulic pressure and elongation effects from gravity.

The theoretical outer surface area to volume ratios were 1711, 1505, 1395 and 1440 m² m⁻³ for the 3, 4-bore and the two 7-bore membranes, respectively, assuming the closest hexagonal packing (Table 2). Here the membrane area was defined using the outer surface because in practice it would be the area of interest. These ratios are considerably higher than conventional flat and tubular membranes, although lower than typical single-bore hollow fibres, for example, one with an outer diameter of 1.5 mm and an area to volume ratio of 2418 m² m⁻³.

3.2. Microstructures of the multi-bore capillary membranes

The multi-bore membranes prepared have an asymmetric micro-structure with micro-channels formed in between the outer and inner surfaces (Fig. 3). The formation of the micro-channels can be described as a spontaneous fingering process driven by the density difference between the coagulant and the ceramic suspension, i.e., the well-recognised Rayleigh-Taylor instability that amplifies interfacial disturbing waves to drive the periodical uneven invasion of a light fluid into a heavy fluid [28–31]. At the beginning of the phase-inversion process when the ceramic suspension contacts water, the outflow of the solvent from the ceramic suspension to water causes the ceramic suspension to contract, and this causes the interface between the ceramic suspension and water to move towards the suspension side with an extremely high acceleration. This acceleration of the interface is the first key factor to initiate the Rayleigh-Taylor instability. As the ceramic suspension is heavier than water, the direction of the inter-facial acceleration points to the heavier fluid, then the secondary requirement for the Rayleigh-Taylor instability is met, thus the fingering process starts and periodical micro-streams of water invade into the ceramic suspension to form micro-channels [28]. After initiation, the micro-channels grow by the momentum of the invading micro-streams and the final length and width of the micro-channels are determined by the complex interplay between the initial acceleration, densities, viscosities, precipitation rate and etc. [28]. Determined by the physical nature of the Rayleigh-Taylor instability, the direction of the micro-channels in general is perpendicular to the surface where it initiates, therefore the arrangement of micro-channels will adapt the configuration of the multi-bore designs and generate different patterns of micro-channels at different regions, as shown in Fig. 3(a-d). During

the micro-channel formation process, when the water micro-streams meet from opposite directions, the momentum would be dissipated, leaving a denser sponge-like layer sandwiched in between the micro-channels in the precursors, which can be completely gas-tight after sintering and serves as another separating layer. These sponge-like layers are important to the mechanical property of the membranes, as a large part of material is distributed here. All of the sintered membranes showed a fully densified outer surface (Fig. 3e). The inner surface showed some surface pores (Fig. 3f), but this doesn't affect the gas tightness since the dense outer surface and the sandwiched dense layer in the membrane walls guarantee the membrane is leak-free.

3.3. Mechanical property of the multi-bore capillary membranes

The multi-bore capillary membranes fabricated from DMSO-based suspension exhibited fracture loads of 10.4, 13.5 and 15.4 N for the 3, 4, and 7-bore membranes, respectively, as shown in Table 3. And for the 7-bore-NMP membrane, the fracture load was 11.7 N. Comparing this to previous studies [11,12,32], the multi-bore membranes showed a significant increase in fracture load to that of single-bore hollow fibre membranes, which are also displayed in Table 3.

The increase in the fracture load is due to the increase in the second moment of area, and the relation is expressed by

$$F = \frac{4I \times \sigma_{max}}{L \times R} \qquad (2)$$

Here F is the fracture load, σ_{max} is the flexural strength which is determined by the material and the microstructure and is irrelevant to the geometry of the sample, R is the radius of the sample, L is the span used during the test. And I is the second moment of area defined by

$$I = \int y^2 dA \qquad (3)$$

y is the coordinate of the force direction relative to the centre of the cross section, and the integral over the solid area of the cross section. Apparently I is geometry dependent. Compared to typical single-bore hollow fibres, the multi-bore membranes in general have much larger solid cross-sectional area and therefore the fracture load will be substantially increased. Using the dimensions listed in Table 2, the second moment of area I of each multi-bore membrane is calculated and listed in Table 3. In general, the trend of the fracture load is concurrent with the trend of the calculated I. For the 7-bore-NMP membrane, I is smaller than the 7-bore-DMSO membrane due to the thinner walls, and therefore has a smaller fracture load. Using Eq. (2), the flexural strengths of the multi-bore membranes are obtained and also listed in Table 3, and they are comparable to the strength given in literature for the single-bore LSCF hollow fibres.

As the multi-bore capillary membranes posed an advantage of exhibiting a fracture load much greater than the single-bore hollow fibre membranes, they can provide possible solutions for the weak mechanical stability problem encountered by the single-bore hollow fibre membranes. Furthermore, multi-bore configurations allow optimised distribution of membrane materials, i.e., the effective separating layer can be designed to be much thinner than single-bore hollow fibres whilst having better mechanical stability. The advantages will be discussed in detail in the following section.

3.4. Oxygen permeation through the multi-bore capillary membranes

Oxygen permeation through the multi-bore capillary membranes was measured at an argon sweep gas flowrate of 100 cm³ min⁻¹ and the effect of operating temperature on the permeation flux was investigated (Fig. 4). As the temperature increased from 750 to 1000 °C, the oxygen permeation flux increased significantly. The oxygen permeation fluxes were in the range of 0.02–0.95, 0.02–1.02 and 0.03–1.03 cm³ cm⁻² min⁻¹ for the 3, 4, 7-bore membranes made from
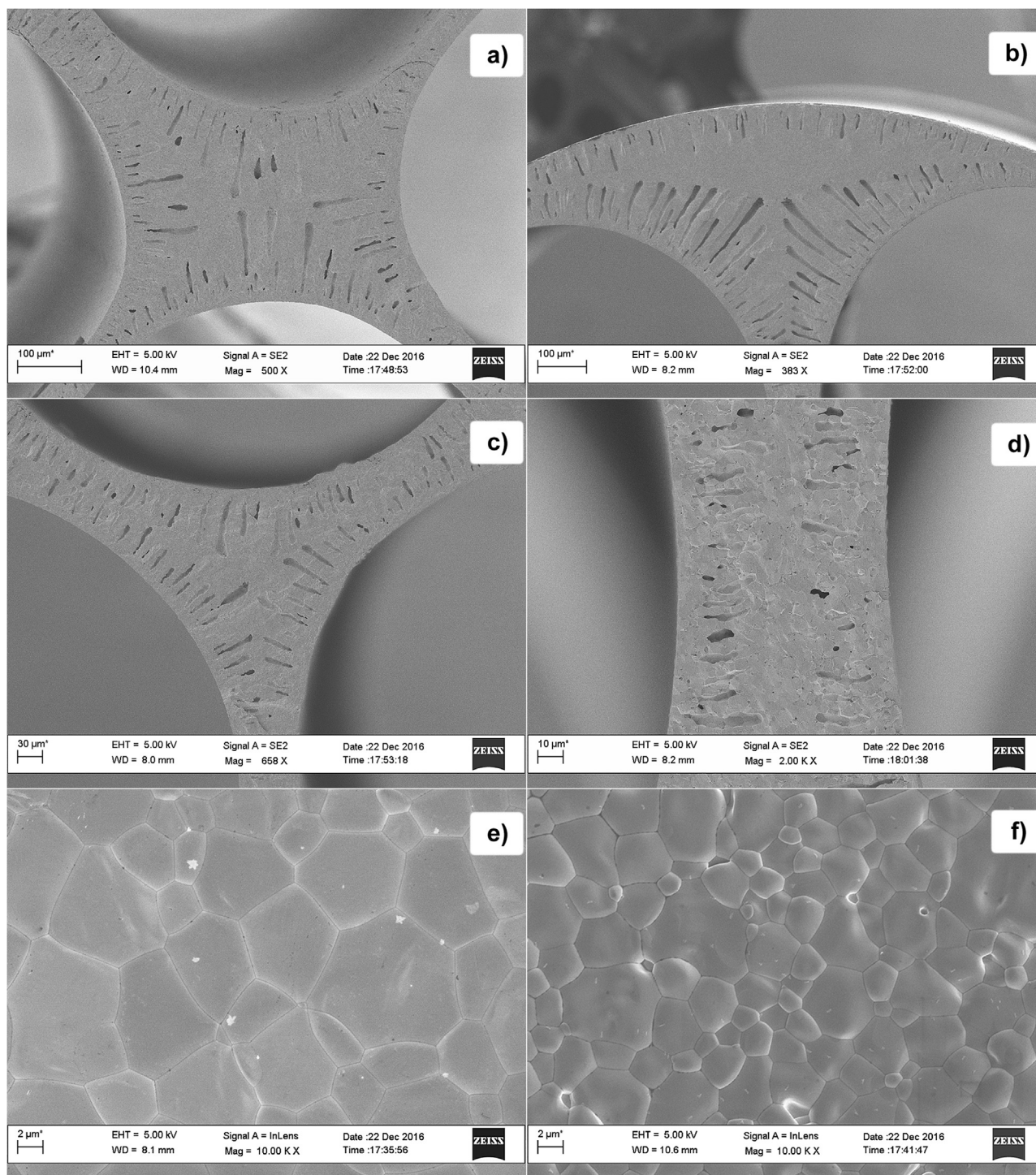
Fig. 3. SEM images showing the microstructure of the multi-bore LSCF membranes. (a) cross section of the central wall in the 4-bore membrane; (b) cross section of the wall between the shell and two bores in the 7-bore-DMSO membrane; (c) cross section of the wall between the central bore and surrounding two bores in the 7-bore-DMSO membrane; (d) cross section of the wall between two bores in the 7-bore-NMP membrane; (e) and (f) are the outer surface and inner surface, respectively.

the DMSO-based suspension, respectively, and 0.03–1.39 cm^3 cm^{-2} min^{-1} for the 7-bore-NMP membrane.

From the results obtained in the current study, there are no obvious differences between the oxygen permeation flux for the four different multi-bore membranes and no correlation between the flux and the cross-sectional morphology can be made at temperatures lower than 900 °C. However, at higher temperatures, it is evident that the 7-bore-NMP membrane, which has the thinnest effective separating layer, climbed faster than others and reached 1.39 cm^3 cm^{-2} min^{-1} at 1000 °C. And in general, from 900 °C to 1000 °C the relative increasing
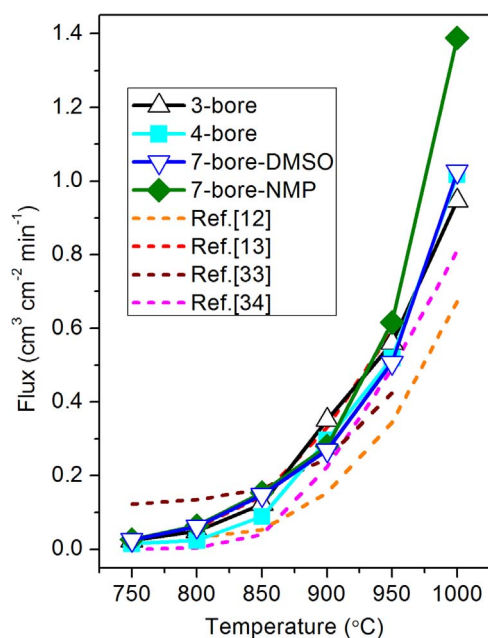
rate of the permeation flux can be related to the effective separating layer thickness, say, the thinner ones increase faster than the thicker ones.

Such a trend can be interpreted by the change in the transport resistance distribution at different temperatures. It is established that oxygen permeation through MIEC membranes can be hypothetically divided into three types of step and accordingly three types of resistance [27]. One is the mass transfer in the gas phase, through which molecular oxygen is adsorbed (desorbed) by (from) the membrane surface. The second type is the reduction/oxidation reactions of

Table 3
Three-point bending test results of LSCF multi-bore membranes and data of single-bore hollow fibres from literature.

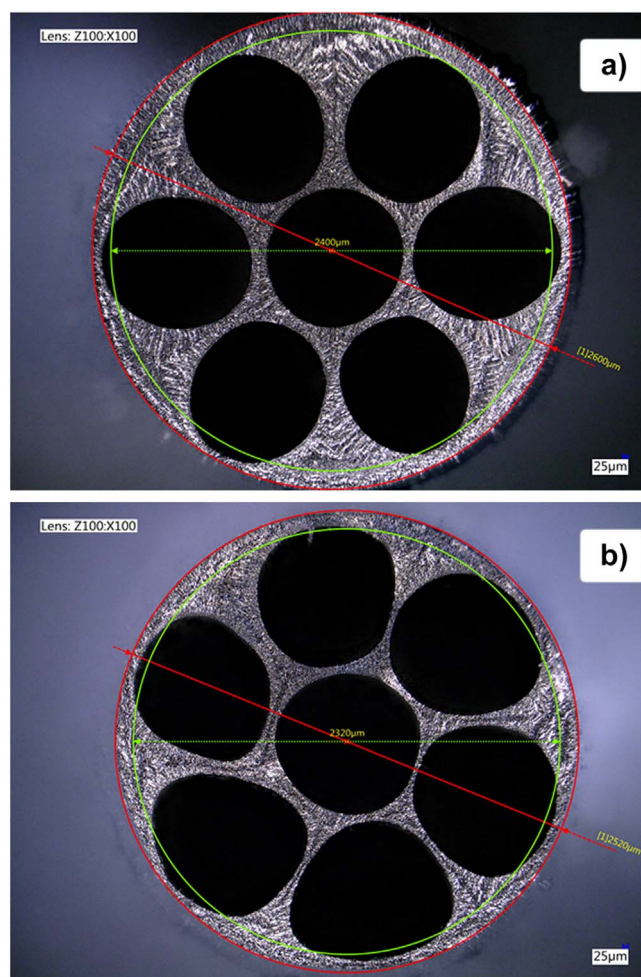| Configuration	Fracture load (N)	Testing span (cm)	Second moment of area (10^{-12} m^4)	Flexural strength (MPa)	Sintering temperature (°C)	Literature
3 – bore capillary	10.4	3	0.7229	113	1350	This work
4 – bore capillary	13.5		1.1608	105		
7 – bore-DMSO capillary	15.4		1.1598	129		
7 – bore-NMP capillary	11.7		0.8498	129		
Single-bore hollow fibre (ID=1.11 mm; OD=1.28 mm)	0.8	5	0.0683[a]	111	1260	[11]
Single-bore hollow fibre (ID=1.18 mm; OD=1.40 mm)	1.2		0.0868[a]	113		
Single-bore hollow fibre (ID=1.08 mm; OD=1.73 mm)	6.0[a]	3.2	0.3729	110	1350	[32]
Single-bore hollow fibre (IDs & ODs not given)	Not given	3.2	–	89–154	1420	[12]

[a] Not given in the literature, but calculated using relevant data in the literature.

Fig. 4. Oxygen permeation flux of multi-bore LSCF membranes and the data of single-bore LSCF hollow fibres from literatures [12,13,33,34].

Fig. 5. Comparison between the effective thickness of the 7-bore-DMSO (a) and 7-bore-NMP (b) membranes. The outer surface is highlighted by the red circle, and the green circle shows the distance 100 μm from the outer surface. The total lengths of the green line within the bores are 2.00 mm for the 7-bore-DMSO membrane and 3.44 mm for the 7-bore-NMP membrane. (For interpretation of the references to color in this figure legend, the reader is referred to the web version of this article.)

oxygen species on the membrane surface, where the adsorbed oxygen molecule is decomposed into oxygen ions and incorporated into surface vacancies, or on the opposite, oxygen ions to oxygen molecules. The second type of step is often called surface exchange. The third type of resistance is the diffusion of oxygen ions in the membrane bulk, which is membrane thickness dependent. The three types of resistance are coupled and any change in one step would lead to changes in others, but the relative importance of each step can be estimated based on kinetic parameters.

When ignoring the resistance from gas phase mass transfer, surface exchange and bulk diffusion become the two major resistances for oxygen permeation, and they are affected by two key parameters of the membrane material, i.e., the surface exchange coefficient k and the chemical diffusion coefficient D. The relative importance of surface exchange and bulk diffusion can then be estimated by a hypothetic critical thickness L_c [35], which is defined by

$$L_c = \frac{D}{k} \tag{4}$$

When the membrane thickness is equal to L_c, the resistances from surface exchange and bulk diffusion are equally important. If the membrane thickness is larger than L_c, the resistance from bulk

diffusion becomes more important, whereas if the membrane is thinner than L_c, surface exchange becomes more important.

k and D of the LSCF material have been studied by different researchers using electrical conductivity relaxation or isotope exchange techniques [36–39]. Here we take the result from Niedrig et al. [38] to estimate the L_c at 800 °C and 900 °C. The L_c of LSCF at 800 °C is
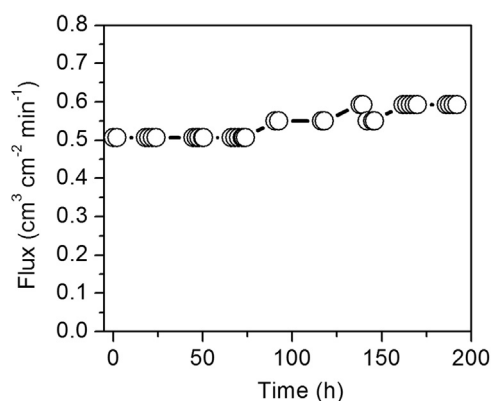
Fig. 6. Oxygen permeation flux of a 7-bore-DMSO membrane at 950 °C for ~200 h.
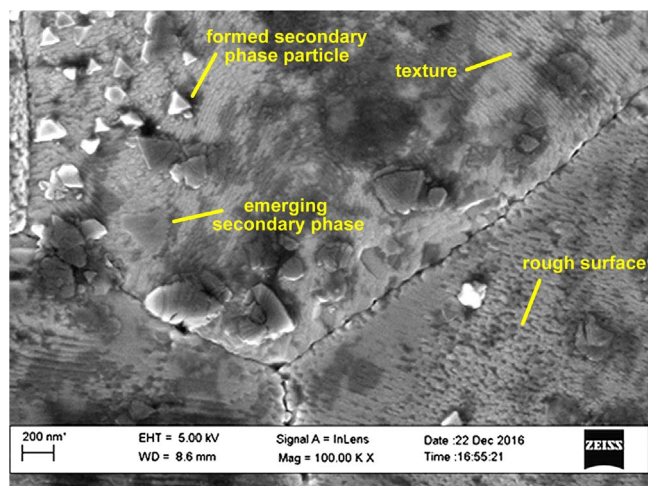

Fig. 7. High-magnification SEM image taken from the outer surface of the 7-bore-DMSO membrane after ~200 h test.

estimated to be above 300 μm, but reduces to less than 100 μm at 900 °C. It can be expected that the L_c will decrease further at higher temperatures if the parameters k and D follow the Arrhenius relation. Xu and Thomson found that, k has much higher activation energy than D for LSCF material [27], therefore k will increase faster than D when the temperature increases, leading to decreasing L_c.

Considering the effective thickness of the multi-bore membranes and single-bore hollow fibres, which is normally thinner than 300 μm, the majority of transport resistance at lower temperatures lies in surface exchange. Normally, the resistance from the permeate side surface is larger than the side exposed to air when the effective surface area of both sides are comparable. This is because the surface exchange coefficient reduces quickly at lower oxygen partial pressures [36–39]. But at higher temperatures, the majority of the transport resistance moves from surface exchange towards bulk diffusion, because in that case, the effective membrane thickness will be considerably larger than L_c. Such transition of the controlling step from surface exchange to bulk diffusion when the temperature increases has been observed in disc LSCF membranes by Xu [27] and in single-bore LSCF hollow fibres by Tan et al. [10], which agreed well with the trend of L_c obtained from the k and D.

Based on the above analysis, the oxygen permeation through the multi-bore LSCF membranes at lower temperatures can be considered to be mainly affected by surface exchange, but at higher temperatures it would be mainly affected by bulk diffusion. Interestingly, despite the effective permeate side membrane area increases with the number of bores, the 3, 4, 7-bore membranes showed similar permeation fluxes at lower temperatures, though theoretically the permeation flux should be roughly proportional to the effective membrane area. And in these

multi-bore membranes, the permeate side oxygen partial pressure for each type of membrane is roughly the same, therefore this deviation from the theoretical prediction is not due to the difference in partial pressure. Aside from surface exchange and bulk diffusion, this deviation can be explained by the resistance from gas phase mass transfer. The aforementioned transport resistance distribution was based on an assumption that the mass transfer in the gas phase is fast enough and the related resistance is negligible. However this assumption is often not true, especially when the membrane is thin and the flux is high. When a sweep gas is used at the permeate side, the oxygen concentration near the membrane surface is always higher than the bulk of the gas phase, due to the boundary layer effect of the fluid. This limits the desorption and removal of oxygen molecules from the permeate side membrane surface, and will have a direct impact on the surface exchange, reducing the exchange rate. The boundary layer effect will then couple with surface exchange to add further transport resistance, when the permeation process is controlled by surface exchange. However, the boundary layer effect can be reduced by increasing the velocity of the sweep gas. Although the total sweep gas flowrate was fixed at 100 cm³ min⁻¹ in this study, the velocities of the sweep gas inside each bore were very different for the multi-bore membranes. Based on the bore diameters listed in Table 2, the sweep gas velocities calculated in the bores were 1.33 m s⁻¹ for the 3-bore membrane, 0.81 m s⁻¹ for the 4-bore membrane, 0.51 and 0.50 m s⁻¹ for the 7-bore-DMSO and 7-bore-NMP membranes. Therefore, it is possible that the membranes with more number of bores (thus greater surface area) to have more severe boundary layer effects (thus slower surface exchange) than the membranes with less number of bores, resulting in no significant permeation differences between the multi-bore membranes.

When the temperature is increased and oxygen permeation is mainly affected by bulk diffusion, the permeation flux will be evidently affected by the thickness of the membrane. The effect of membrane thickness can be recognised directly from the two 7-bore LSCF membranes since they have the same sweep gas velocities during the test. The permeation flux of the 7-bore-NMP membrane is 35% higher than the 7-bore-DMSO membrane, which is a direct reflection of the reduced effective membrane thickness. To make the comparison between the effective thicknesses clearer, in Fig. 5, the two 7-bore membranes are compared by drawing a green circle that is 100 μm from the outer surface, a distance roughly equals to the critical thickness L_c of LSCF at 900 °C. The total length of the walls that are thinner than 100 μm is represented by the green lines located inside the bores, which is 3.44 mm for the 7-bore-NMP membrane and 2.00 mm for the 7-bore-DMSO membrane. This suggests the 7-bore-NMP membrane has lower resistance when the permeation is dominated by bulk diffusion, which is in line with the higher oxygen permeation obtained for the 7-bore-NMP membrane at temperatures above 900 °C.

The oxygen permeation fluxes obtained from the multi-bore LSCF membranes are also compared with literature values of the single-bore LSCF hollow fibre membranes, and the values from literature [12,13,33,34] are plotted in Fig. 4. To make fair comparisons, the single-bore hollow fibres were selected to have a sandwich-like wall structure, which is similar to the wall structure of the multi-bore membranes. It is apparent that the multi-bore membranes have higher permeation fluxes than the single-bore hollow fibres at 1000 °C. And it is also worthy to mention, the permeation fluxes of single-bore hollow fibres in literature are all based on an effective membrane area rather than the outer surface area, which could overestimate the permeation flux by 20% compared to the flux based on the outer surface. Taking this into account, at 1000 °C, the permeation flux of the 7-bore-NMP membrane is 214% of the flux of a single-bore hollow fibre from Tan *et. al.,* [34].
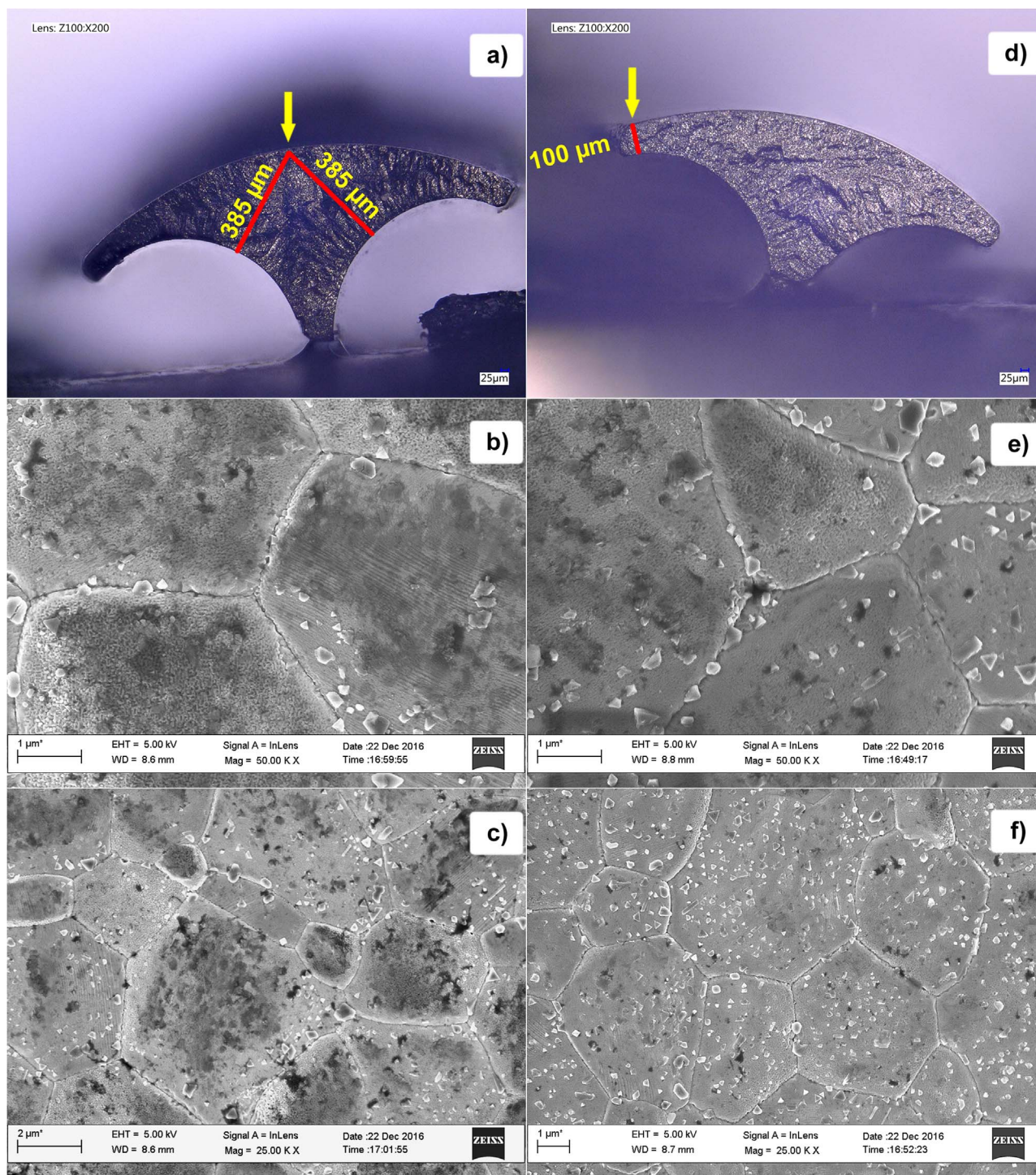
Fig. 8. Images of two sites on the outer surface of the 7-bore-DMSO membrane after ~200 h test. Left column display (a) a digital microscope picture showing the site of interest by the arrow and (b and c) SEM images taken from the site. Right column display (d) a digital microscope picture showing the other site of interest and (e and f) SEM images taken from the site.

3.5. Performance and structural stabilities

One concern of MIEC membranes is their performance and structural stability during operation. It has been long noticed that MIEC membranes such as BSCF and LSCF undergo material degradation when an oxygen chemical potential gradient is applied across the membrane at high temperatures [40–43], which can be described as kinetic demixing or decomposition. It happens because cations in the membrane material tend to diffuse from the low oxygen partial pressure side toward the high oxygen partial pressure side, as required by the Gibbs-Duhem relation, and the whole membrane wall will also move towards the high oxygen partial pressure side. If cations diffuse with different diffusion coefficients, the membrane material will be demixed from the previous homogenous composition [44,45].

To study this aspect of multi-bore MIEC membranes, a LSCF 7-bore-DMSO membrane was tested at 950 °C for about 200 h and was characterized. Fig. 6 depicts the permeation flux over the 200 h period and it shows a slight increasing trend. This slight increase was also observed in our previous 1128-h and 5512-h long-term tests with single-bore LSCF hollow fibre membrane modules, during which the

oxygen permeation flux increased slightly at the initial few hundred hours, but it was then stable for the rest of the operation [42,43].

After the 200-h test, the membrane was examined by SEM. In Fig. 7, a high magnification image of the outer surface reveals significant changes compared with untested samples. It can be seen that the surface became rough after the long-term test, and texture structure can also be found on the surface, whereas untested samples show a very smooth texture-free surface. The roughened surface might be the consequence of diffusion of cations from the permeate side to the air side, which led to morphological instabilities and changed the initial smooth surface [45]. Such morphological instabilities led by diffusion have also been widely observed in other material systems [45]. Other than the roughened surface, it is notable that bright particles of secondary phases are scattered on the surface, mostly in a regular triangle shape. Some darker particles with similar shapes appear to emerge from the membrane surface, suggesting the bright secondary phase particles were grown from the membrane surface and the darker particles are at their early stage of the growth. The size of these secondary phase particles is smaller than 200 nm, which is much smaller than the resolution of Energy Dispersive Spectrum (EDS) analysis and therefore the chemical composition could not be determined. However, in our previous long-term test of LSCF membranes, secondary phase particles with same triangle shape were also found on the air side surface, and they were big enough to be determined by EDS analysis, which confirmed that they are mainly cobalt oxides [42]. The growth of cobalt oxides is the result of kinetic decomposition. It has been determined by secondary ion mass spectrometry (SIMS) analysis that cobalt ions has the highest diffusivity in the LSCF material [43], and will be enriched the most on the air side membrane surface. The LSCF composition will then enter into a thermodynamically unstable region, leading to the decomposition of LSCF material and the generation of new cobalt oxides phase. It perhaps was the changes in the morphology and chemical composition that led to the slight increase in oxygen permeation flux over the 200-h test as shown in Fig. 6. The roughened morphology would lead to higher surface area and the higher cobalt content would increase surface oxygen vacancy, which can all lead to faster surface oxygen exchange at the feed side and reduce the overall transport resistance. Compared to the outer surface, no considerable changes were observed on the inner surface of the membrane, which is concurrent with the previous studies, and it can be attributed to the self-limiting cation diffusion process at the permeate side due to the deficient A-site vacancies in the perovskite lattice [43].

A morphological comparison is made between two different sites on the outer membrane surface after the long-term test. The two sites are indicated in Fig. 8(a and d). One site is located at the thick wall, where the distance from the site to the nearest inner surface is 385 µm; and the other site is located at the thin wall, where the membrane thickness is 100 µm. Both sites showed similar morphologies with roughened surfaces and scattered secondary phase particles, but the number of the secondary phase particles for the thinner wall is obviously larger than the thicker wall (Fig. 8(b, c and e, f)). This result reflects the difference in the driving force for cation diffusion at varied positions in multi-bore membranes. As in kinetic demixing/decomposition, cation diffusion is affected by oxygen chemical potential gradient across the membrane following the Gibbs–Duhem relation [45], the diffusion rate will be faster when the gradient is steeper. In the multi-bore membrane, the oxygen partial pressure difference between the air side and the permeate side is the same for different sites, and the chemical potential gradient is inversely proportional to the membrane thickness, hence the thinner part would have steeper chemical potential gradient than the thicker part to drive the cations faster, and therefore formed more secondary phase particles on the outer surface. This phenomenon indicates that after long-term operation, the thinnest wall will undergo most serious material degradation, and failure of the membrane will most likely to happen at the thinnest walls. It is worthy to mention that

in our spinneret designs, the inhomogeneity in the wall thickness increases with the number of the bores, and the 3- and 4-bore membranes have thicker walls than the 7-bore membrane, which indicates they will show slower degradation at the thinnest walls and thus longer operation lifetime. Therefore, by using different multi-bore designs, it is possible to achieve the balance between mechanical stability, permeation flux and material degradation to meet the needs in different applications.

4. Conclusion

The mixed ionic-electronic conducting LSCF multi-bore capillary membranes with 3, 4 and 7 bores were successfully fabricated using the combined phase inversion and sintering technique. The membranes fabricated have an asymmetric structure with micro-channels formed in between the outer and inner bore surfaces. Meanwhile, a dense layer is sandwiched in between the micro-channels. An advantage of the multi-bore geometries was the enhancement in mechanical property, where it exhibited fracture loads much higher than single-bore hollow fibre membranes. The oxygen permeation flux of the multi-bore membranes showed similar results to that of the LSCF single-bore hollow fibres with similar asymmetric structures at temperatures lower than 900 ºC, but it became considerably higher than the single-bore hollow fibres at higher temperatures. It is argued that the multi-bore configurations can realise optimised material distributions to achieve both high permeation flux and robust mechanical property. Furthermore, long-term test suggested that the thinnest separating walls in multi-bore membranes would undergo fastest material degradation, and therefore they would be the limiting step in determining the operation lifetime.

References

[1] H.J.M. Bouwmeester, A.J. Burggraaf, Dense ceramic membranes for oxygen separation, in: P.J. Gellings, H.J.M. Bouwmeester (Eds.), The CRC Handbook Of Solid State Electrochemistry, CRC Press, 1997.
[2] P.V. Hendriksen, P.H. Larsen, M. Mogensen, F.W. Poulsen, K. Wiik, Prospects and problems of dense oxygen permeable membranes, Catal. Today 56 (2000) 283–295.
[3] J. Sunarso, S. Baumann, J.M. Serra, W.A. Meulenberg, S. Liu, Y.S. Lin, J.C. Diniz da Costa, Mixed ionic-electronic conducting (MIEC) ceramic-based membranes for oxygen separation, J. Membr. Sci. 320 (2008) 13–41.
[4] Y. Teraoka, H.M. Zhang, S. Furukawa, N. Yamazoe, Oxygen permeation through perovskite-type oxides, Chem. Lett. (1985) 1743–1746.
[5] C.-s. Chen, S.-j. Feng, S. Ran, D.-c. Zhu, W. Liu, H.J.M. Bouwmeester, Conversion of methane to syngas by a membrane-based oxidation–reforming process, Angew. Chem. Int. Ed. 42 (2003) 5196–5198.
[6] X. Dong, W. Jin, N. Xu, K. Li, Dense ceramic catalytic membranes and membrane reactors for energy and environmental applications, Chem. Commun. 47 (2011) 10886–10902.
[7] N.H. Othman, Z. Wu, K. Li, A micro-structured La0.6Sr0.4Co0.2Fe0.8O3−δ hollow fibre membrane reactor for oxidative coupling of methane, J. Membr. Sci. 468 (2014) 31–41.
[8] Z. Shao, H. Dong, G. Xiong, Y. Cong, W. Yang, Performance of a mixed-conducting ceramic membrane reactor with high oxygen permeability for methane conversion, J. Membr. Sci. 183 (2001) 181–192.
[9] H. Wang, Y. Cong, W. Yang, Investigation on the partial oxidation of methane to syngas in a tubular Ba0.5Sr0.5Co0.8Fe0.2O3−δ membrane reactor, Catal. Today 82 (2003) 157–166.
[10] X. Tan, Y. Liu, K. Li, Mixed conducting ceramic hollow-fiber membranes for air separation, AIChE J. 51 (2005) 1991–2000.
[11] B. Zydorczak, Z. Wu, K. Li, Fabrication of ultrathin La0.6Sr0.4Co0.2Fe0.8O3−δ hollow fibre membranes for oxygen permeation, Chem. Eng. Sci. 64 (2009) 4383–4388.
[12] X. Tan, N. Liu, B. Meng, S. Liu, Morphology control of the perovskite hollow fibre membranes for oxygen separation using different bore fluids, J. Membr. Sci. 378 (2011) 308–318.
[13] D. Han, J. Sunarso, X. Tan, Z. Yan, L. Liu, S. Liu, Optimizing oxygen transport

through La0.6Sr0.4Co0.2Fe0.8O3−δHollow fiber by microstructure modification and Ag/Pt catalyst deposition, Energy Fuels 26 (2012) 4728–4734.

[14] T. Schiestel, M. Kilgus, S. Peter, K.J. Caspary, H. Wang, J. Caro, Hollow fibre perovskite membranes for oxygen separation, J. Membr. Sci. 258 (2005) 1–4.

[15] H. Jiang, H. Wang, S. Werth, T. Schiestel, J. Caro, Simultaneous production of hydrogen and synthesis gas by combining water splitting with partial oxidation of methane in a hollow-fiber membrane reactor, Angew. Chem. Int. Ed. 47 (2008) 9341–9344.

[16] H. Wang, S. Werth, T. Schiestel, J. Caro, Perovskite hollow-fiber membranes for the production of oxygen-enriched air, Angew. Chem. Int. Ed. 44 (2005) 6906–6909.

[17] R. An, J. Song, Y. Li, X. Tan, J. Sunarso, C. Zhang, S. Wang, S. Liu, Bundling strategy to simultaneously improve the mechanical strength and oxygen permeation flux of the individual perovskite hollow fiber membranes, J. Membr. Sci. 527 (2017) 137–142.

[18] J. Zhu, Z. Liu, S. Guo, W. Jin, Influence of permeation modes on oxygen permeability of the multichannel mixed-conducting hollow fibre membrane, Chem. Eng. Sci. 122 (2015) 614–621.

[19] J. Zhu, S. Guo, Z. Zhang, X. Jiang, Z. Liu, W. Jin, CO2-tolerant mixed-conducting multichannel hollow fiber membrane for efficient oxygen separation, J. Membr. Sci. 485 (2015) 79–86.

[20] J. Zhu, S. Guo, G. Liu, Z. Liu, Z. Zhang, W. Jin, A robust mixed-conducting multichannel hollow fiber membrane reactor, AlChE J. 61 (2015) 2592–2599.

[21] J. Zhu, Z. Dong, Z. Liu, K. Zhang, G. Zhang, W. Jin, Multichannel mixed-conducting hollow fiber membranes for oxygen separation, AlChE J. 60 (2014) 1969–1976.

[22] M. Lee, Z. Wu, B. Wang, K. Li, Micro-structured alumina multi-channel capillary tubes and monoliths, J. Membr. Sci. (2015).

[23] F. Iguchi, N. Sata, H. Yugami, H. Takamura, Oxygen permeation properties and the stability of La$_{0.6}$Sr$_{0.4}$Fe$_{0.8}$Co$_{0.2}$O$_3$ studied by Raman spectroscopy, Solid State Ion. 177 (2006) 2281–2284.

[24] J.A. Lane, S.J. Benson, D. Waller, J.A. Kilner, Oxygen transport in La$_{0.6}$Sr$_{0.4}$Co$_{0.2}$Fe$_{0.8}$O$_{3-δ}$, Solid State Ion. 121 (1999) 201–208.

[25] S.P. Scott, D. Mantzavinos, A. Hartley, M. Sahibzada, I.S. Metcalfe, Reactivity of LSCF perovskites, Solid State Ion. 152 (2002) 777–781.

[26] S.J. Xu, W.J. Thomson, Stability of La$_{0.6}$Sr$_{0.4}$Co$_{0.2}$Fe$_{0.8}$O$_{3-δ}$ perovskite membranes in reducing and nonreducing environments, Ind. Eng. Chem. Res. 37 (1998) 1290–1299.

[27] S.J. Xu, W.J. Thomson, Oxygen permeation rates through ion-conducting perovskite membranes, Chem. Eng. Sci. 54 (1999) 3839–3850.

[28] M. Lee, B. Wang, Z. Wu, K. Li, Formation of micro-channels in ceramic membranes – Spatial structure, simulation, and potential use in water treatment, J. Membr. Sci. 483 (2015) 1–14.

[29] D.J. Lewis, The Instability of Liquid Surfaces when Accelerated in a Direction Perpendicular to their Planes. II, Proceedings of the Royal Society of London. Series A. Mathematical and Physical Sciences, vol. 202, 1950, pp. 81–96.

[30] D.H. Sharp, An overview of Rayleigh-Taylor instability, Physica D: Nonlinear Phenom. 12 (1984) 3–18.

[31] G. Taylor, The Instability of Liquid Surfaces when Accelerated in a Direction Perpendicular to their Planes. I, Proceedings of the Royal Society of London. Series A. Mathematical and Physical Sciences, vol. 201, 1950, pp. 192–196.

[32] X. Tan, Z. Wang, K. Li, Effects of sintering on the properties of La0.6Sr0.4Co0.2Fe0.8O3−δ Perovskite hollow fiber membranes, Ind. Eng. Chem. Res. 49 (2010) 2895–2901.

[33] C. Yacou, J. Sunarso, C.X.C. Lin, S. Smart, S. Liu, J.C. Diniz da Costa, Palladium surface modified La0.6Sr0.4Co0.2Fe0.8O3−δ hollow fibres for oxygen separation, J. Membr. Sci. 380 (2011) 223–231.

[34] X. Tan, Z. Wang, H. Liu, S. Liu, Enhancement of oxygen permeation through La0.6Sr0.4Co0.2Fe0.8O3−δ hollow fibre membranes by surface modifications, J. Membr. Sci. 324 (2008) 128–135.

[35] H.J.M. Bouwmeester, H. Kruidhof, A.J. Burggraaf, Importance of the surface exchange kinetics as rate limiting step in oxygen permeation through mixed-conducting oxides, Solid State Ion. 72 (1994) 185–194.

[36] H.J.M. Bouwmeester, M.W. Den Otter, B.A. Boukamp, Oxygen transport in La$_{0.6}$Sr$_{0.4}$Co$_{0.2}$Fe$_{0.8}$O$_{3-δ}$, J. Solid State Electrochem. 8 (2004) 599–605.

[37] Y. Li, K. Gerdes, T. Horita, X. Liu, Surface exchange and bulk diffusivity of LSCF as SOFC cathode: electrical conductivity relaxation and isotope exchange characterizations, J. Electrochem. Soc. 160 (2013) F343–F350.

[38] C. Niedrig, S.F. Wagner, W. Menesklou, S. Baumann, E. Ivers-Tiffée, Oxygen equilibration kinetics of mixed-conducting perovskites BSCF, LSCF, and PSCF at 900°C determined by electrical conductivity relaxation, Solid State Ion. 283 (2015) 30–37.

[39] J.A. Lane, J.A. Kilner, Measuring oxygen diffusion and oxygen surface exchange by conductivity relaxation, Solid State Ion. 136–137 (2000) 997–1001.

[40] H.L. Lein, K. Wiik, T. Grande, Kinetic demixing and decomposition of oxygen permeable membranes, Solid State Ion. 177 (2006) 1587–1590.

[41] R.H.E. van Doorn, H.J.M. Bouwmeester, A.J. Burggraaf, Kinetic decomposition of La$_{0.3}$Sr$_{0.7}$CoO$_{3-δ}$ perovskite membranes during oxygen permeation, Solid State Ion. 111 (1998) 263–272.

[42] B. Wang, B. Zydorczak, Z.T. Wu, K. Li, Stabilities of La$_{0.6}$Sr$_{0.4}$Co$_{0.2}$Fe$_{0.8}$O$_{3-δ}$ oxygen separation membranes-effects of kinetic demixing/decomposition and impurity segregation, J. Membr. Sci. 344 (2009) 101–106.

[43] B. Wang, B. Zydorczak, D. Poulidi, I.S. Metcalfe, K. Li, A further investigation of the kinetic demixing/decomposition of La0.6Sr0.4Co0.2Fe0.8O3−δ oxygen separation membranes, J. Membr. Sci. 369 (2011) 526–535.

[44] H. Schmalzried, W. Laqua, Multicomponent oxides in oxygen potential gradients, Oxid. Met. 15 (1981) 339–353.

[45] M. Martin, Materials in thermodynamic potential gradients, J. Chem. Thermodyn. 35 (2003) 1291–1308.